Advances in Applied Mathematics and Mechanics
Adv. Appl. Math. Mech., Vol. **8**, No. 1, pp. 37-51

DOI: 10.4208/aamm.2014.m512
February 2016

Improving the Stability of the Multiple-Relaxation-Time Lattice Boltzmann Method by a Viscosity Counteracting Approach

Chunze Zhang, Yongguang Cheng*, Shan Huang and Jiayang Wu

State Key Laboratory of Water Resources and Hydropower Engineering Science, Wuhan University, Wuhan 430072, China

Received 20 February 2014; Accepted (in revised version) 28 November 2014

Abstract. Numerical instability may occur when simulating high Reynolds number flows by the lattice Boltzmann method (LBM). The multiple-relaxation-time (MRT) model of the LBM can improve the accuracy and stability, but is still subject to numerical instability when simulating flows with large single-grid Reynolds number (Reynolds number/grid number). The viscosity counteracting approach proposed recently is a method of enhancing the stability of the LBM. However, its effectiveness was only verified in the single-relaxation-time model of the LBM (SRT-LBM). This paper aims to propose the viscosity counteracting approach for the multiple-relaxation-time model (MRT-LBM) and analyze its numerical characteristics. The verification is conducted by simulating some benchmark cases: the two-dimensional (2D) lid-driven cavity flow, Poiseuille flow, Taylor-Green vortex flow and Couette flow, and three-dimensional (3D) rectangular jet. Qualitative and Quantitative comparisons show that the viscosity counteracting approach for the MRT-LBM has better accuracy and stability than that for the SRT-LBM.

AMS subject classifications: 65M10, 78A48

Key words: Multiple-relaxation-time lattice Boltzmann method, viscosity counteracting, high Reynolds number flow, Poiseuille flow, Couette flow, Taylor-Green vortex flow, lid-driven cavity flow.

1 Introduction

The lattice Boltzmann method (LBM) has some unique advantages for simulating various complex flow problems [1]. Among many models of the LBM, the single-relaxation-time (SRT) model (with the Bhatnagar-Gross-Krook collision operator) has been popular because it has a simpler collision term [2]. However, this model becomes unstable when

*Corresponding author.
Email: ygcheng@whu.edu.cn (Y. G. Cheng)

simulating high Reynolds-number flows [3]. Many efforts have been made to improve the stability of the LBM. Hou improved the robustness of the SRT model by introducing a large eddy model for turbulence simulations [4]. He proposed a multi-grid method that imposes curvilinear coordinates near the boundary walls to increase the Reynolds number in simulated problems [5]. Zhang improved the numerical stability by introducing fractional volume in the LBM [6]. Shu suggested a step-by-step LBM that combines the standard LBM with the fractional step method [7]. A significant improvement of the accuracy and stability of LBM was not achieved until the establishment of the multiple-relaxation-time (MRT) model [8], which was theoretically analyzed in detail by Lallemand and Luo in 2000 [9]. In the MRT model, the collision process is conducted in the moment spaces, and different relaxation times correspond to different physical variables. The numerical stability and accuracy of MRT model is much better than other lattice Boltzmann models [10, 14, 21], and the model provides much richer physical information of the fluid field. According to some reports, the simulation costs are 15% higher than the SRT model, but the stability and accuracy benefits override the computational expense [11]. The MRT model has been widely used to simulate flows, especially flows of high Reynolds number [12–14]. However, the MRT model becomes unstable when the single-grid Reynolds number is very high if no additional effort, such as the subgrid-scale modeling, is adopted [15].

Recently, a viscosity counteracting approach (VC) was proposed by Cheng et al. for improving stability of the SRT-model in simulations of high Reynolds number flows [16]. The main idea is to counteract the artificial viscosity corresponding to a flow of greater viscosity introduced intentionally to simulate an actual flow with smaller viscosity in a stable way by adding an external foring term to the equations. The enhanced stability and accuracy of this approach were verified on typical benchmarks. There are still rooms for improving its effectiveness. Because the approach works well for SRT-LBM and MRT model has better stability and accuracy than SRT model, one may anticipate that better performance can be achieved by introducing the viscosity counteracting approach into MRT model.

The aim of this study is to develop a viscosity counteracting approach for the MRT-LBM and verify its effectiveness. Section 2 describes the basic theory of the MRT model and the principles of the proposed approach. Section 3 addresses the verification of the approach by some benchmarks: 2D Poiseuille flow, Couette flow, Taylor-Green vortex flow and lid-driven cavity flow, and 3D rectangular jet. Section 4 concludes the paper.

2 Methods

2.1 Multiple-relaxation-time model

Without loss of generality, we consider the two-dimensional-nine-velocity (D2Q9) model

with an MRT collision operator [9]:

$$f_\alpha(\boldsymbol{x}+\boldsymbol{e}_\alpha\delta_t,t+\delta_t)=f_\alpha(\boldsymbol{x},t)-\boldsymbol{M}^{-1}\hat{\boldsymbol{S}}[\boldsymbol{m}_\alpha(\mathbf{x},t)-\boldsymbol{m}_\alpha^{eq}(\mathbf{x},t)]+\delta_t F_\alpha,\quad \alpha=0,1,\cdots,8, \tag{2.1}$$

where $\{f_\alpha(\boldsymbol{x},t):\alpha=0,1,\cdots,8\}$ are the discrete distribution functions at position $\boldsymbol{x}$ and time t. The discrete velocities $\{\boldsymbol{e}_\alpha:\alpha=0,1,\cdots,8\}$ are defined by $\boldsymbol{e}_0=(0,0)$, $\boldsymbol{e}_1=-\boldsymbol{e}_3=(1,0)c$, $\boldsymbol{e}_2=-\boldsymbol{e}_4=(0,1)c$, $\boldsymbol{e}_5=-\boldsymbol{e}_7=(1,1)c$, and $\boldsymbol{e}_6=-\boldsymbol{e}_8=(-1,1)c$. Here, $c=\delta x/\delta t$, δx is the lattice spacing and δt is the time step. The distribution and the equilibrium distribution functions in the moment space are given by $\{\boldsymbol{m}_\alpha(\boldsymbol{x},t):\alpha=0,1,\cdots,8\}$ and $\{\boldsymbol{m}_\alpha^{eq}(\boldsymbol{x},t):\alpha=0,1,\cdots,8\}$, respectively. $\boldsymbol{M}$ is the transformation matrix, $\hat{\boldsymbol{S}}$ is the non-negative diagonal matrix, and $\{F_\alpha:\alpha=0,1,\cdots,8\}$ are the forcing terms accounting for a body force $\boldsymbol{F}$. In the D2Q9 model, $\boldsymbol{M}$ is given by

$$\begin{pmatrix} 1 & 1 & 1 & 1 & 1 & 1 & 1 & 1 & 1 \\ -4 & -1 & -1 & -1 & -1 & 2 & 2 & 2 & 2 \\ 4 & -2 & -2 & -2 & -2 & 1 & 1 & 1 & 1 \\ 0 & 1 & 0 & -1 & 0 & 1 & -1 & -1 & 1 \\ 0 & -2 & 0 & 2 & 0 & 1 & -1 & -1 & 1 \\ 0 & 0 & 0 & 0 & -1 & 1 & 1 & -1 & -1 \\ 0 & 0 & -2 & 0 & 2 & 1 & 1 & -1 & -1 \\ 0 & 1 & -1 & 1 & -1 & 0 & 0 & 0 & 0 \\ 0 & 0 & 0 & 0 & 0 & 1 & -1 & 1 & -1 \end{pmatrix}. \tag{2.2}$$

The equilibrium distribution functions in the moment space $\boldsymbol{m}^{eq}$ are

$$\boldsymbol{m}^{eq}=\rho\left(1,-2+3\boldsymbol{u}^2,1-3\boldsymbol{u}^2,u_x,-u_x,u_y,-u_y,u_x^2-u_y^2,u_xu_y\right)^T. \tag{2.3}$$

The relaxation transform matrix $\hat{\boldsymbol{S}}$ is

$$\hat{\boldsymbol{S}}=\mathrm{diag}\left(s_\rho,s_e,s_\varepsilon,s_\chi,s_q,s_\chi,s_q,s_\nu,s_\nu\right). \tag{2.4}$$

Similar expressions of D3Q19 model can be referenced to [11, 14, 21]. In Section 3, the relaxation parameters for 2D test cases, are given as $s_\rho=s_\varepsilon=s_\chi=1.0$, $s_e=s_q=1.2$, while s_ν are determined according to kinematic viscosity; for 3D test case, they follow reference [14]. How the forcing term is introduced strongly influences the performance of the method mentioned in the next section. Since the counteracted viscosity term is of second-order accuracy, the numerical treatment of the forcing term must be at least second-order accurate. Otherwise, second-order dissipations may affect the simulation results. The force term of LBE proposed by Cheng et al. [17] is adopted, which can be written as

$$F_\alpha=\frac{1}{2}[g_\alpha(\boldsymbol{x},t)+g_\alpha(\boldsymbol{x}+\boldsymbol{e}_\alpha\delta_t,t+\delta_t)], \tag{2.5}$$

where $g_\alpha(\boldsymbol{x},t)$ in Eq. (2.5) is given by

$$g_\alpha=\omega_\alpha\left\{A+\boldsymbol{F}\cdot\left[\frac{(\boldsymbol{e}_\alpha-\boldsymbol{u})}{c_s^2}+\frac{(\boldsymbol{e}_\alpha\cdot\boldsymbol{u})\boldsymbol{e}_\alpha}{c_s^4}\right]\right\}, \tag{2.6}$$

in which $\boldsymbol{u}$ is velocity, w_α is the weighting parameters: $\omega_0=4/9$, $\omega_{1-4}=1/9$, $\omega_{5-8}=1/36$, A is the source term in the fluid continuity equation, here $A=0$, and $\boldsymbol{F}$ is the external forcing term for the momentum equation. For steady flow or changing slowly unsteady flow, the next time step $g_\alpha(\boldsymbol{x}+\boldsymbol{e}_\alpha\delta_t,t+\delta_t)$ may be computed as $g_\alpha(\boldsymbol{x}+\boldsymbol{e}_\alpha\delta_t,t)$ for simplicity. The density ρ and the velocity $\boldsymbol{u}$ are defined as

$$\rho=\sum_\alpha f_\alpha,\quad \rho\boldsymbol{u}=\sum_\alpha \boldsymbol{e}_\alpha f_\alpha. \tag{2.7}$$

2.2 Viscosity counteracting approach

When simulating high Reynolds number flows, instabilities arise from small dissipation at low viscosity. The viscosity term in the Navier-Stokes (N-S) equations involves a second-order derivative, which plays a dissipation role that maintains the numerical stability. In numerical simulations of the N-S equations, higher-order truncation errors also play a vital role in maintaining the stability and the accuracy. The widely used LBM models are second order in space, and may be rendered more stable by modifying the third or higher-order truncation error terms without affecting the convergence rate. In addition, we all know that the relaxation time τ cannot be smaller than 0.5, i.e., the viscosity in LBM cannot be smaller than 0. However, in the computing process with a low viscosity, the viscosity error may be negative due to the numerical error, which is one of the reasons for numerical instability [16]. Therefore, we may add an extra viscosity term in the N-S equations, as shown in Eq. (2.8), which is later canceled out by treating it as an external forcing term [16]

$$\frac{\partial(\rho u_i)}{\partial t}+\frac{\partial(\rho u_i u_j)}{\partial x_j}=-\frac{\partial p}{\partial x_i}+(\nu+\nu_c)\frac{\partial}{\partial x_j}(2\rho S_{ij})-\nu_c\frac{\partial}{\partial x_j}(2\rho S_{ij}). \tag{2.8}$$

On the right side of Eq. (2.8), the $(\nu+\nu_c)$ in the second term is the viscosity specified in the simulation (applied viscosity), and ν_c is the viscosity to be counteracted (counteracted viscosity). The difference between them is the desired simulation viscosity ν (target viscosity). In the viscosity counteracting approach, the external force F_i is given by

$$F_i=-\nu_c\frac{\partial(2\rho S_{ij})}{\partial x_i}, \tag{2.9}$$

where

$$S_{ij}=\frac{1}{2}\Big(\frac{\partial u_i}{\partial x_j}+\frac{\partial u_j}{\partial x_i}\Big)$$

is the strain rate tensor. The calculation of Eq. (2.9) should also be second order accurate or higher. S_{ij} can be calculated from the non-equilibrium part of the distribution function:

$$S_{ij}=\frac{3s_\nu}{2\rho}\sum_{\alpha=1}^{b}[f_\alpha-f_\alpha^{eq}]e_{\alpha i}e_{\alpha j}, \tag{2.10}$$

where s_ν is the relaxation factor corresponding to the applied viscosity, i.e.,

$$s_\nu = 1/(3(\nu+\nu_c)+0.5). \tag{2.11}$$

The partial derivatives of S_{ij} may be obtained by a finite-difference scheme of forth-order accuracy:

$$\frac{\partial \phi}{\partial \boldsymbol{x}} = \frac{-\phi_{i+2}+8\phi_{i+1}-8\phi_{i-1}+\phi_{i-2}}{12\delta_x}. \tag{2.12}$$

It should be noted that, for the nodes at the boundary vicinity, the partial derivatives of S_{ij} may be calculated by extrapolation methods. Using the above viscosity counteracting approach, we can improve the stability of MRT-based simulation. Stability can be enforced by artificially specifying the applied viscosity based on numerical experimentation. To limit the errors in the result to an acceptable range, the applied viscosity should not be very large.

3 Verifications

Three 2D benchmarks including Poiseuille flow, Couette flow and Taylor-Green vortex flow are simulated to verify the effectiveness and accuracy of the MRT-VC scheme, and 2D lid-driven cavity flow and 3D rectangular jet are presented to prove that MRT-VC has better accuracy and stability than MRT-LBM and SRT-VC.

3.1 Poiseuille flow

The analytical solution of Poiseuille flow is [18,19]

$$u_x^*(y) = U_0\Big(1-\frac{(2y-N_y)^2}{N_y^2}\Big), \quad u_y^*(x,y) = 0, \tag{3.1a}$$

$$p_1^* - p_2^* = 8\rho\nu U_0 \frac{N_x}{N_y^2}, \tag{3.1b}$$

where U_0 is the maximum velocity along the central line, p_1 and p_2 are the inlet and outlet pressures, and the superscript $*$ denotes the analytical values. At both sides, the inlet velocity profile $u_x(0,y) = u_x^*(y)$ and the outlet pressure $p_2 = p_2^* = 1.0$ are specified. At the lower and upper wall, the nonslip condition is imposed. The two-dimensional rectangular region is discretized into a mesh of $N_x \times N_y$ nodes, where N_x and N_y are the lattice node numbers. We specify $N_x = 2N_y$, $N_y = 10$,20, and 40, and $U_0 = 0.1$. Without the viscosity counteraction, the lowest stable viscosity attained by SRT and MRT models is just around 0.02 and 0.01, respectively. Using the MRT-based viscosity counteracting approach (denoted as MRT-VC), we can simulate small target viscosities such as 0.01, 0.005, 0.002, 0.001, and 0.000, by setting the applied viscosity to 0.02, the corresponding counteracted viscosity are 0.01, 0.015, 0.018, 0.019, 0.2. Under identical conditions, we can also

Table 1: Comparison of viscosity errors in Poiseuille flow simulated by MRT-VC and SRT-VC.

N_y	Method	$\nu=0.01$	$\nu=0.005$	$\nu=0.002$	$\nu=0.001$	$\nu=0.000$
10	MRT−VC	$4.153e^{-6}$	$1.042e^{-5}$	$2.920e^{-5}$	$4.138e^{-5}$	$7.277e^{-5}$
	SRT−VC	$3.352e^{-4}$	$5.353e^{-4}$	$7.105e^{-4}$	$7.843e^{-4}$	$8.731e^{-4}$
20	MRT−VC	$4.022e^{-6}$	$5.176e^{-6}$	$7.688e^{-6}$	$8.257e^{-6}$	$3.103e^{-5}$
	SRT−VC	$1.956e^{-4}$	$3.207e^{-4}$	$4.452e^{-4}$	$5.208e^{-4}$	$5.953e^{-4}$

simulate these small viscosity cases by the SRT-based viscosity counteracting approach (denoted as SRT-VC) for comparison between the two methods. From the simulated results of Poiseuille flow, we obtain the resulting viscosity ν' through solving Eq. (3.1b), in which the inlet pressure is given as the simulated value. By analyzing the errors in $|\nu'-\nu|$, the difference between the resulting viscosity and the target viscosity, we can evaluate the characteristics of the viscosity errors in both methods. Table 1 compares the viscosity errors between MRT-VC and SRT-VC. The magnitude of the error in MRT-VC is around 10^{-6} to 10^{-5}, while that in SRT-VC is around 10^{-4}, indicating that the former is more accurate than the latter.

To analyze the convergence features of MRT-VC, we simulate the Poiseuille problem on different mesh sizes. Fig. 1 plots the spatial convergence curves of the error in velocity. The velocity error here is defined as the maximum relative velocity error in the whole flow field, given as

$$E_{um}=\max\left(\sqrt{(u_x-u_x^*)^2+(u_y-u_y^*)^2}/U_0\right).$$

Fig. 1 excludes the case of $\nu=0.000$ in mesh size $N_y=40$, which is unstable unless the relaxation factor matrix is altered. The curves for $\nu=0.001$ to 0.01 show that the spatial convergence of MRT-VC is second order, indicating that MRT-VC preserves the second-order spatial accuracy of LBM.

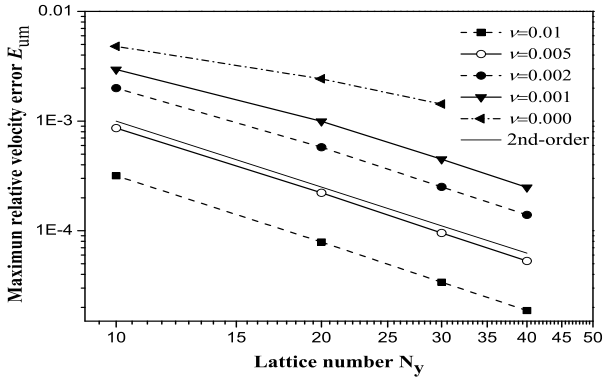

Figure 1: Spatial convergence characteristics of velocity error in Poiseuille flow simulated by MRT-VC.

3.2 Couette flow

Couette flow is simulated to test whether MRT-VC can handle strong shearing transient flows. The rectangular region is also discretized as a $N_x \times N_y$ lattice. Initially, the flow is stationary with velocity $u(x,y,0)=0$ and pressure $p(x,y,0)=p_0$. Periodic boundary conditions are applied on the left and right sides of the simulation domain. Velocity boundary condition $u=U_0$ is applied on the bottom, and nonslip condition is applied on the top. The analytical velocity profile is given by [19]:

$$u_x^*(y,t)=U_0\Big(1-\frac{y}{N_y}\Big)-\sum_{i=1}^{\infty}\Big[\frac{2U_0}{i\pi}\sin\Big(i\pi\frac{y}{N_y}\Big)\exp\Big(-i^2\pi^2\frac{\nu\cdot t}{N_y^2}\Big)\Big], \tag{3.2a}$$

$$u_y^*=0. \tag{3.2b}$$

The lattice size is fixed as $N_x \times N_y = 100\times 100$, and the parameters are as follows: the bottom velocity $U_0=0.1$, the applied viscosity 0.01, the target viscosity $\nu=$ 0.005,0.001,0.0005, and 0.0001, the corresponding counteracted viscosity are 0.005, 0.009, 0.0095, 0.0099. Table 2 lists the E_{um} errors of MRT-VC and SRT-VC at various ν and $\nu\cdot t$, where E_{um} is the maximum relative velocity error in the whole field, defined in Section 3.1. It is noticed that the errors increase as the target viscosity ν decreases (the counteracted viscosity ν_c increases), and decrease as $\nu\cdot t$ increases. MRT-VC yields smaller error than SRT-VC. At $\nu\cdot t=1$, the errors by MRT-VC are only 1/3 to 1/2 of those of SRT-VC. As $\nu\cdot t$ increases to 50, the error ratios reduce to 1/5 to 1/3. The significant error reduction of MRT-VC relative to SRT-VC for transient Couette flow demonstrates that MRT-VC can properly capture sharp velocity gradient transition (or large flow shearing). Fig. 2 plots the velocity convergence curves as functions of time in MRT-VC simulations of Couette flow. In the case of $\nu\cdot t$ larger 5 or ν larger than 0.0005, the convergence rate is approximately first order, revealing that MRT-VC guarantees the first-order temporal accuracy of LBM.

Table 2: Velocity errors for the 2D Couette flow simulated by MRT-VC and SRT-VC comparing with analytical values.

$\nu\cdot t$	Method	$\nu=0.005$	$\nu=0.001$	$\nu=0.0005$	$\nu=0.0001$
c	MRT−VC	0.01005	0.05626	0.08672	0.19559
	SRT−VC	0.03573	0.12336	0.18242	0.33936
5	MRT−VC	0.00193	0.01469	0.02808	0.09085
	SRT−VC	0.00906	0.05248	0.08611	0.19536
10	MRT−VC	0.00095	0.00770	0.01540	0.05764
	SRT−VC	0.00480	0.03119	0.05467	0.14453
50	MRT−VC	0.00019	0.00161	0.00339	0.01660
	SRT−VC	0.00100	0.00770	0.01515	0.05612

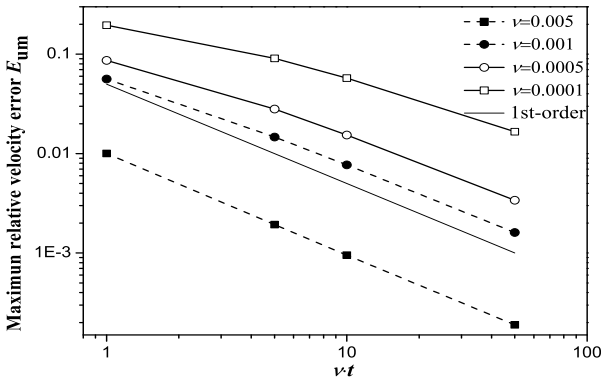

Figure 2: Temporal convergence characteristics of velocity error in Couette flow simulated by MRT-VC.

3.3 Taylor-Green vortex flow

To analyze the influence of wave number on the stability of MRT-VC, the method is tested on Taylor-Green vortex flows. The analytical solutions of this flow obtained from the 2D incompressible N-S equations are as follows:

$$u_x^*(x,y,t) = -U_0 \cos\left(k\cdot 2\pi\frac{x}{N}\right)\sin\left(k\cdot 2\pi\frac{y}{N}\right)\exp(-2k^2\nu t), \tag{3.3a}$$

$$u_y^*(x,y,t) = U_0 \sin\left(k\cdot 2\pi\frac{x}{N}\right)\cos\left(k\cdot 2\pi\frac{y}{N}\right)\exp(-2k^2\nu t), \tag{3.3b}$$

where U_0 is the magnitude of the initial velocity, ν is the shear viscosity, k is the wave number, and N is the domain size. Simulations of this decaying vortex phenomenon are conducted on a $N_x \times N_y = N^2 = 100^2$ lattice with periodic boundary conditions at all four sides. Selected parameters are $U_0 = 0.1$ and $k = 1,2,\cdots,10$. After many trial-and-error simulations, we have identified critical viscosities for stable vortices, i.e., the smallest viscosities at which the vortices maintain their initial shapes throughout 10000 LBM steps. We apply the four LBM methods: MRT, SRT, MRT-VC, and SRT-VC, and compare their critical viscosities at different wave numbers. As shown in Fig. 3, the critical viscosities are very small for $k = 1,2$, and 10, and relative larger for $k = 3$ to 9. Compared with MRT and SRT, MRT-VC and SRT-VC approach can yield smaller critical viscosities. In addition, the critical viscosities identified in MRT-VC are smaller than those in SRT-VC. This suggests that MRT-VC is more stable than SRT-VC.

3.4 Lid-driven cavity flow

To test whether MRT-VC can simulate high Reynolds number complex vortex flows with good accuracy and stability, we apply it to the lid-driven cavity problem. The velocity $U_0 = 0.1$ is specified on the top boundary and nonslip condition is used on the bottom and the two sides. First, we used a 100×100 lattice to simulate $Re = 5000$ flow, which needs the

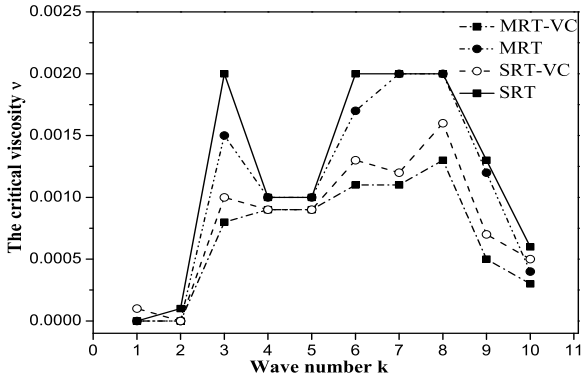

Figure 3: Comparison of critical viscosities at different wave numbers in Taylor-Green vortex flow simulated by four LBM methods.

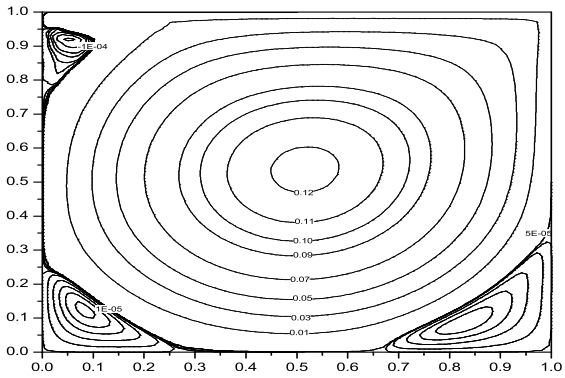

Figure 4: Streamlines of the lid-driven cavity flow at $Re=5000$ simulated by MRT-VC.

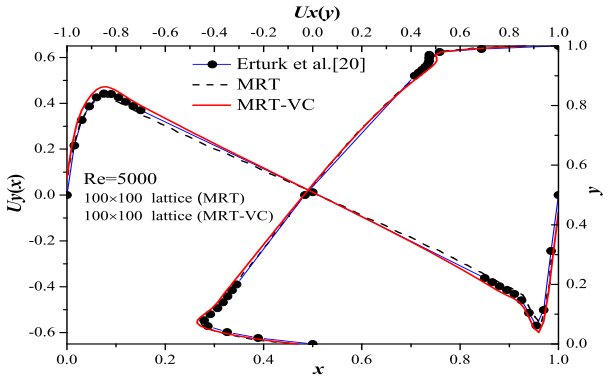

Figure 5: Comparison of axial velocity profiles of the lid-driven cavity flow at $Re=5000$.

target viscosity of 0.002. Both MRT and MRT-VC yield stable results while SRT simulation is divergent. The viscosity counteracting approach assume an applied viscosity of 0.003. Fig. 4 shows the streamlines of the lid-driven cavity flow at $Re=5000$ generated by MRT-

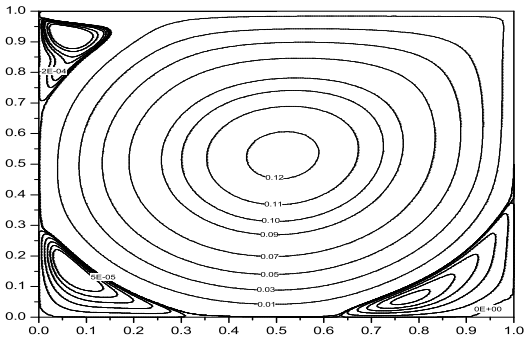

Figure 6: Streamlines of the lid-driven cavity flow at $Re=10000$ simulated by MRT-VC.

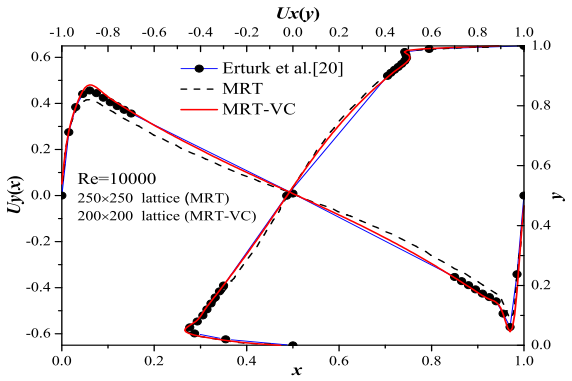

Figure 7: Comparison of the axial velocity profiles of the lid-driven cavity flow at $Re=10000$.

VC. Fig. 5 shows the velocity profiles along the central axes. Apparently, the results of MRT-VC and MRT are almost the same, and both are consistent with the reference data [20]. Next, we simulate the lid-driven cavity flow at $Re=10000$. The parameters are unchanged, but the lattice is doubled to 200×200. Not only SRT but also MRT are unstable in this case. MRT-VC with applied viscosity of 0.003 is stable and yield the results in Fig. 6 and Fig. 7. The MRT curves in Fig. 7 are obtained on a finer lattice of 250×250. Apparently, the results obtained by MRT-VC are consistent with those obtained by the fine-mesh high-order scheme in reference [20]. The centers of the primary and secondary vortices for $Re=5000$ and 10000 flows are quantitatively compared in Table 3,

Table 3: Locations of the vortex foci of the lid-driven cavity flow.

Re	Method	Vortex focus locations (x,y)			
		Main vortex	Top left	Bottom left	Bottom right
5000	Present	(0.515, 0.536)	(0.059, 0.909)	(0.070, 0.132)	(0.810, 0.070)
	Erturk [20]	(0.515, 0.535)	(0.063, 0.910)	(0.073, 0.137)	(0.805, 0.073)
10000	Present	(0.512, 0.530)	(0.076, 0.904)	(0.074, 0.154)	(0.782, 0.058)
	Erturk [20]	(0.512, 0.530)	(0.072, 0.912)	(0.058, 0.163)	(0.777, 0.060)

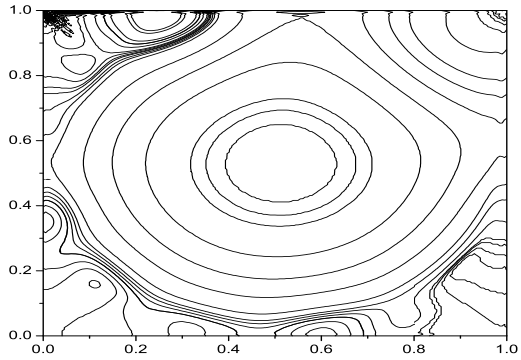

Figure 8: Pressure distribution of the lid-driven cavity flow at $Re=10000$ simulated by MRT-VC at the steady state.

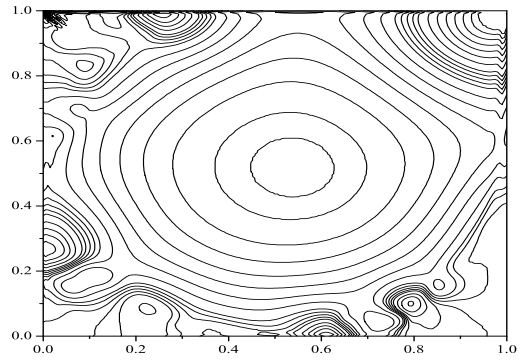

Figure 9: Pressure distribution of the lid-driven cavity flow at $Re=20000$ simulated by MRT-VC at a certain moment.

which also shows the accuracy of MRT-VC. To visualize the source of instability, we plot the pressure distribution in Fig. 8, and focus on the upper left corner, where instability is typically initiated by strong shearing. Rough zigzag patterns appear in the contours of this corner, but are restricted to a small magnitude. These results demonstrate that MRT-VC can simulate large Reynolds number flow on a coarser lattice while maintaining accuracy and stability.

To further verify that MRT-VC enhances numerical stability, we increase the flow Reynolds number to $Re=20000$ on a 200×200 lattice by letting the target viscosity 0.001 and other parameters unchanged. Under these conditions, the flow becomes turbulent and more subordinate vortices appear, consistent with existing reports [20]. The vortices evolve and move within their own cycles, and no instability occur. Fig. 9 shows the pressure distribution at a particular time instant. The pressure contours are smooth except for a very limited rough region in the upper left corner, indicating strong numerical stability there. In addition, using MRT-VC and a 200×200 lattice, we can simulate the flow with $Re=60000$ or even larger. However, due to the lack of data for comparison, we do not

present these results.

3.5 Three-dimensional (3D) rectangular jet

The 3D rectangular jet is simulated to test the effect of MRT-VC for 3D turbulence flow. Fig. 10 depicts the schematic configuration and coordinate system of the flow field. U_0 is jet velocity; U_c is the mean velocity on the jet axis; h_y and h_z are the velocity half-width in the $y-$ and $z-$ directions, respectively. The velocity half-width denotes that the distance between the jet axis and the point which velocity is equal to a half of the mean velocity on the jet axis. The computational domain of the flow field is a rectangular duct ($\Omega = W \times H \times L$). The air issues into the duct from a rectangular orifice ($A = w \times h$) for which the equivalent diameter can be expressed as $De = 2\sqrt{wh/\pi}$. Reynolds number is calculated from height (h), velocity (U_0) and kinematic viscosity of air (ν). We set the initial and boundary conditions by the reference [21]: the whole velocity field is initialized as zero; the jet orifice is set as uniform velocity boundary; Periodic boundary conditions are applied in both $y-$ and $z-$ directions. Like in the literature [22], the physical and lattice parameters are listed in Table 4.

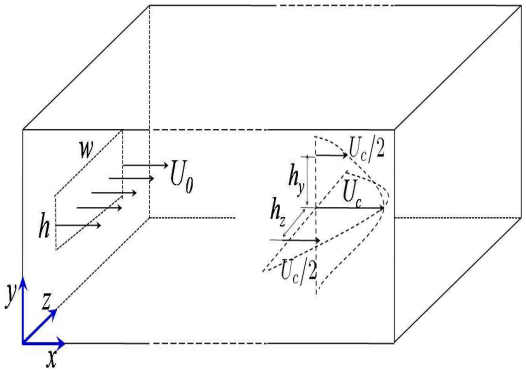

Figure 10: Schematic configuration and coordinate system for the rectangular jet flow.

According our test, with the same mesh and boundary conditions, the MRT-LBM fails to simulate the $Re = 15000$ case because of instability and divergence. Therefore, only the results simulated by MRT-VC is presented. The target viscosity is set as 0.00009, and the applied viscosity is 0.001. The velocity half-width and turbulence intensity are presented and compared with the experimental data. Fig. 11 illustrates the development of the normalized velocity half-width on the $y-$ and $z-$ directions along the jet centerline. The

Table 4: Computational parameters of the rectangular jet case.

	AR (w/h)	Re	U_0	A=$w \times h$	De	$\Omega = W \times H \times L$
Physical unit	5	15000	23(m/s)	0.05×0.01 (m)	0.025(m)	$0.1 \times 0.042 \times 0.032$(m)
Lattice unit			0.1	70×14	35	$150 \times 60 \times 450$

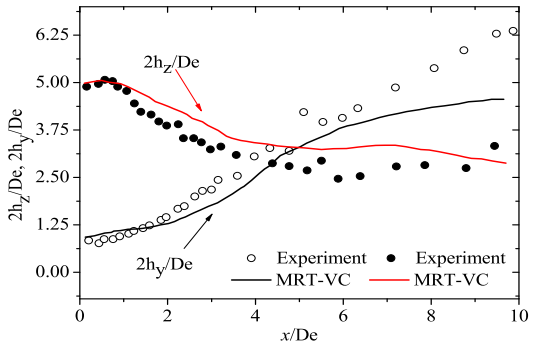

Figure 11: Development of the normalized velocity half-width on the $y-$ and $z-$ directions along the jet centerline.

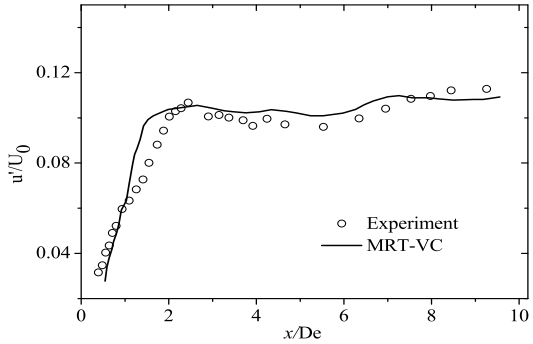

Figure 12: Streamwise turbulence intensity u'/U_0 along the jet centerline.

h_y increases monotonically, which indicates the jet rapidly mixing and spreading along the $y-$ direction. Meanwhile, for the large aspect ratio ($w/h=5.0$) jet, the h_z decreases at early stages and then stays nearly constant. Although the simulated results are not well agreement with the experiment values, the general trends are captured. Fig. 12 shows the streamwise turbulence intensity (u'/U_0) along the jet centerline. The curve increases rapidly near the jet orifice where severe local shear leads to high turbulence, and then, it stay near a constant at the later stages. For this trend, the simulated results yield a better agreement with the experiment data.

It should be noted that, for this case, the highest Reynolds number successfully simulated by MRT-LBM is less than 4000. The performance indicates that, MRT-VC makes an obvious improvement over MRT-LBM.

4 Conclusions

We have proposed a viscosity counteracting approach in order to enhance the stability of the lattice Boltzmann method (LBM) for simulating high Reynolds number flows. The

basic idea is to stabilize the simulation by adding an extra viscosity term, and then removing it through a counteracting external forcing term. The effectiveness and accuracy of the viscosity counteracting approach in the multiple-relaxation-time (MRT) model are verified by simulations of benchmark problems: 2D Poiseuille, Couette, Taylor-Green vortex and lid-driven cavity flows, and 3D rectangular jet. Evidently, this approach improves numerical stability of the MRT model at higher single-grid Reynolds number. The approach is more beneficial for the MRT-LBM than the SRT-LBM. To ensure accuracy, the forcing term must be treated by a second or higher order scheme. The approach preserves the original accuracy of the LBM: second order in space and first order in time. Although the approach adds some computational expense to the LBM, the extra cost is partially offset by the reduced number of grid nodes to simulate the same flow. While this preliminary study has demonstrated the feasibility of the approach, its intrinsic mechanism is not yet clear and should be investigated in a future study.

Acknowledgments

This work was supported by the National Natural Science Foundation of China (NSFC, Grant Numbers 10572106, 10872153 and 11172219) and the Specialized Research Fund for the Doctoral Program of Higher Education of China (Grant No. 20130141110013).

References

[1] S. Y. Chen and G. D. Doolen, *Lattice Boltzmann method for fluid flows,* Annu. Rev. Fluid. Mech., 30 (1998), pp. 329–364.
[2] Y. H. Qian, D. D'Humières and P. Lallemand, *Lattice BGK models for Navier-Stokes equation,* EPL-Europhys. Lett., 17 (1992), pp. 479.
[3] J. D. Sterling and S. Y. Chen, *Stability analysis of lattice Boltzmann methods*, J. Comput. Phys., 123 (1996), pp. 196–206.
[4] S. Hou, J. Sterling and S. Chen, *A lattice Boltzmann subgrid model for high Reynolds number flows,* Pattern Formation and Lattice Gas Automata, 6 (1996), pp. 151–166.
[5] X. Y. He and G. D. Doolen, *Lattice Boltzmann method on curvilinear coordinates system: flow around a circular cylinder,* J. Comput. Phys., 134 (1997), pp. 306–315.
[6] R. Y. Zhang, H. D. Chen and Y. H. Qian, *Effective volumetric lattice Boltzmann scheme,* Phys. Rev. E, 63 (2001), 56705.
[7] C. Shu, X. D. Niu and Y. T. Chew, *A fractional step lattice Boltzmann method for simulating high Reynolds number flows*, Math. Comput. Simulat., 72 (2006), pp. 201–205.
[8] D. Humieres, *Generalized lattice Boltzmann equations,* Rarefied Gas Dynamics-Theory and Simulations, (1994), pp. 450–458.
[9] P. Lallemand and L. S. Luo, *Theory of the lattice Boltzmann method: Dispersion, dissipation, isotropy, Galilean invariance, and stability*, Phys. Rev. E, 61 (2000), 6546.
[10] L. S. Luo, W. Liao and X. W. Chen, *Numerics of the lattice Boltzmann method: effects of collision models on the lattice Boltzmann simulations,* Phys. Rev. E, 83 (2011), 056710.

[11] D. HUMIÈRES, *Multiple-relaxation-time lattice Boltzmann models in three dimensions,* Philos. T. R. Soc. A, 360 (2002), pp. 437–451.
[12] M. KRAFCZYK, J. TÖLKE AND L. S. LUO, *Large-eddy simulations with a multiple-relaxation-time LBE model,* Int. J. Mod. Phys. B, 17 (2003), pp. 33–39.
[13] L. S. LUO, M. KRAFCZYK AND W. SHYY, *Lattice Boltzmann method for computational fluid dynamics,* Encyclopedia of Aerospace Engineering, 2010.
[14] H. D. YU, L. S. LUO AND S. S. GIRIMAJI, *LES of turbulent square jet flow using an MRT lattice Boltzmann model,* Comput. Fluids, 35 (2006), pp. 957–965.
[15] K. N. PREMNATH, M. J. PATTISON AND S. BANERJEE, *Generalized lattice Boltzmann equation with forcing term for computation of wall-bounded turbulent flows,* Phys. Rev. E, 79 (2009), 026703.
[16] Y. G. CHENG AND H. ZHANG, *A viscosity counteracting approach in the lattice Boltzmann BGK model for low viscosity flow: Preliminary verification,* Comput. Math. Appl., 61 (2011), pp. 3690–3702.
[17] Y. G. CHENG AND J. P. LI, *Introducing unsteady non-uniform source terms into the lattice Boltzmann model,* Int. J. Number. Meth. Fluid, 56 (2008), pp. 629–641.
[18] X. Y. HE, Q. S. ZOU AND L. S. LUO, *Analytic solutions of simple flows and analysis of nonslip boundary conditions for the lattice Boltzmann BGK model,* J. Stat. Phys., 87 (1997), pp. 115–136.
[19] C. POZRIKIDIS AND J. H. FERZIGER, *Introduction to theoretical and computational fluid dynamics,* Phys. Today, 50 (1997), 72.
[20] E. ERTURK, T. C. CORKE AND C. GÖKÇÖL, *Numerical solutions of 2-D steady incompressible driven cavity flow at high Reynolds numbers,* Int. J. Numer. Meth. Fluid., 48 (2005), pp. 747–774.
[21] H. D. YU, S. SHARATH AND GIRIMAJI, *Near-field turbulent simulations of rectangular jets using lattice Boltzmann method,* Phys. Fluids, 17 (2005), 125106.
[22] Y. TSUCHIYA AND C. HORIKOSHI, *On the spread of rectangular jets,* Exp. Fluids, 4 (1986), pp. 197–204.